Electromagnetic and Thermal Simulations of Experimentally-Verified B1 shimming Scheme with Local SAR Constrains

L. Tang[1], and T. S. Ibrahim[2]

[1]School of Electrical and Computer Engineering, University of Oklahoma, [2]Departments of Bioengineering and Radiology, Univeristy of Pittsburgh, Pittsburgh, Pennsylvania, United States

Introduction: High and ultrahigh field MRI provide the potential for increased signal to noise ratio (SNR) [1], however, imaging at these field strengths also requires an increased Larmor (operating) frequency and significantly shorter wavelength in tissue. This leads to inhomogeneous B_1^+ field and potentially increased radiofrequency (RF) power requirements (local and global SARs) and thus excessive tissue heating (temperature elevation.) In this work, using 3D numerical simulations and verifications with a 7T scanner equipped with a transmit array system we conduct a comprehensive study using B_1 shimming for potential 7T whole-body applications. Different from previous works [2], this study includes the optimizations of the B_1^+ field, local/average SAR and the resulting temperature elevation in the tissue.

Methods: An anatomically detailed 40-tissue human body mesh obtained from visible human project (http://www.brooks.af.mil/AFRL) was used for simulating the specific absorption rate (SAR) and temperature elevations with a 32-element TEM body-array at 7T [2]. Pancreas organ and one axial slab with 84mm thickness were selected as our targeted regions of interest (ROI). The B_1 shimming scheme was applied to improve the homogeneity of the B_1^+ field in ROIs while minimizing 1) total (in the while body) RF power absorption and the 2) local SAR peaks (anywhere in the body including the arms). The temperature changes were then calculated.

A 3D bio-heat model of the body was made to compute the temperature changes due to RF power deposition caused by 7T MRI operation. Bio-heat equation and the boundary condition [3], as shown in Equations (1) and (2), were applied in the temperature simulations.

$$\rho C_p \frac{\partial T}{\partial t} = K\nabla^2 T + A_0 - B(T - T_b) + \rho SAR \quad (1) \qquad K\frac{\partial T}{\partial n}(x,y,z) = -H_a(T_{x,y,z} - T_a) \quad (2)$$

Temperature changes caused by the RF power deposition were computed using Equation (1), where the spatial resolution is 6mm and the time step is set 0.46seconds. The human body model (37 ºC) was put into cool environment (24 ºC) until equilibrium condition (dT/dt = 2 × 10^{-7} °C/s for 30 minutes) was met. The SAR values (due to quadrature excitation and B_1 shimming) were then applied in order to obtain the corresponding temperature elevation.

Experimental Verification: To validate the simulations including the capability for calculating the coupling between the coil elements and the improved B_1 shimming scheme with constrains on both the local and average SARs, an experiment was performed on a comparable 8-element TEM coil at 7T. Using a spherical phantom (17.5 cm in diameter) as the coil load, experiments and simulations were performed to utilize the B_1 shimming aimed at increasing B_1^+ field intensity in the ROI (a region that exhibited low B_1^+ field intensity during quadrature excitation) with minimization of the local and average SARs over the whole volume of the phantom. The experiments were conducted with an 8-channel transmit array system and directly utilized phases and amplitudes obtained from the simulations (***no B_1^+ field measurements were performed***). Figure 1 shows the comparison of the simulations and experimental results. The results show an a very good agreement, where the B_1^+ field intensity in the 3D ROI was increased by 4 folds (when compared to quadrature excitation at the same input RF power) and was obtained with successful minimization of 1) local SARs, 2) global SARs, and 3) the variation in the B_1^+ distribution. The 4.5 μT represents the maximum B_1^+ intensity inside the selected ROI where the local SAR was below 8 W/Kg per 1gm, and the average SAR was approximately 2 W/Kg.

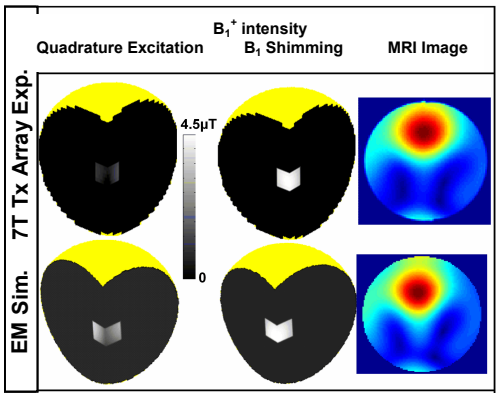

Figure 1. 7 tesla high intensity, localized, and homogeneous 3D B_1 shimming without B_1 measurements on a phantom with brain-like properties. The electromagnetic simulations which achieved successful minimization of 1) actual local SARs (under 8 W/Kg/gm), 2) global SARs (under 4 W/Kg), and 3) the variations (under 0.1 coefficient of variation) in the B_1^+ distribution was validated with Tx array experiment.

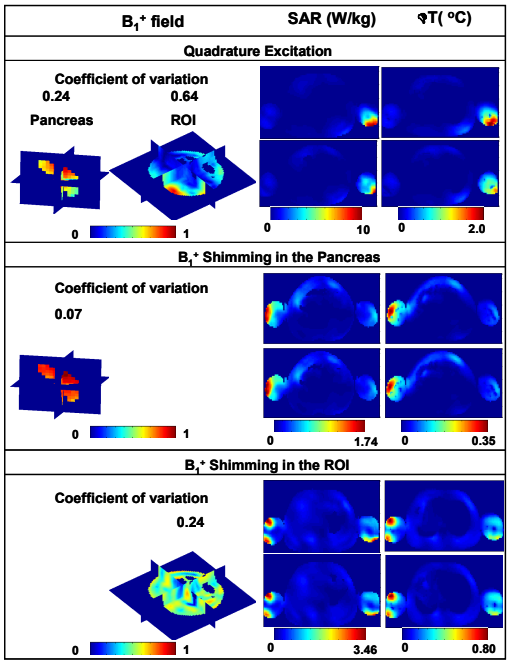

Figure 2. The B_1^+ field, and SAR (averaged over any 10 gram of tissue) and the temperature elevation (ΔT) distributions within whole body under quadrature excitation and B_1 shimming targeted for minimization of 1) actual local SARs (under 10 W/Kg/gm), 2) global SARs (under 4 W/Kg), and 3) the variations in the B_1^+ distribution at 7 tesla.

Results and Conclusions: Figure 2 displays the B_1^+ field and SAR distributions, and the temperature elevations ΔT in the whole-body anatomical model under quadrature and the B_1^+ shimming excitations. The 3D subfigures show the B_1^+ field homogeneity improvement; the two 2D figures show the comparison between the SAR and ΔT distributions at planes where the maximum ΔT occurs (the top row under each excitation condition) and the plane where the maximum SAR occurs (the bottom row under each excitation condition). The distributions of the SAR and ΔT in the same plane have similar patterns under each excitation condition. The close spatial correlation between the SAR and ΔT distribution is because that the highest SARs or temperature elevations are located at the arms where the tissue components are relatively simple (i.e. mostly muscles) and the variation of the tissues thermal properties is minor. In this case, the temperature changes primarily depend on the amount of the deposited RF power. Figure 2 also demonstrates reduced temperature elevation by the improved B_1^+ shimming scheme. Such results also support the notion that minimizing local SARs is probably sufficient for satisfying the requirements on temperature elevations.

Acknowledgements: **NIH 1R01EB00984, ADRC, Siemens**

References: [1] C. N. Chen et al, *MRM,* vol. 3, pp. 722-729, 1986.
[2] R. Abraham et al, *MRM,* vol. 57, pp. 235-242, 2007. [3] J. Wang et al, *IEEE Trans. Micro. Theo. Tech.*, vol. 47, pp. 1528-1534, 1999.